Synchrotron x-ray study of dimensional crossover in solid-phase smectic liquid-crystal films

D. Y. Noh, J. D. Brock,* J. O. Fossum,† J. P. Hill, W. J. Nuttall, J. D. Litster, and R. J. Birgeneau
Department of Physics, Massachusetts Institute of Technology, Cambridge, Massachusetts 02139
(Received 23 April 1990; revised manuscript received 9 August 1990)

The crystalline phases of the liquid crystal 8OSI [racemic 4-(2'-methylbutyl)phenyl 4'-(octyloxy)-(1,1')-biphenyl-4-carboxylate] have been studied using high-resolution synchrotron x-ray-scattering techniques. A careful analysis has been performed on the x-ray-scattering profiles of samples with thicknesses varying from 1000 molecular layers to five layers. Three-dimensional long-range positional order with large-amplitude thermal fluctuations is observed for a very thick film. As the thickness is decreased, two-dimensional characteristics become apparent. The scattering profiles of thin films are described by the power-law line shape, $1/|\mathbf{Q}-\mathbf{G}|^{2-\eta_{\rm eff}}$, with an effective exponent $\eta_{\rm eff}$, which evolves with thickness.

I. INTRODUCTION

Because of their large thermal fluctuations, two-dimensional (2D) systems show quite different behavior from those in three dimensions. Three-dimensional (3D) solids exhibit true long-range positional order; that is, the constituent particles vibrate around well-defined 3D lattice positions with an amplitude which is small compared to the interparticle spacing. On the other hand, broken translational symmetry is impossible for two-dimensional systems because of the overwhelming amplitude of the phonon excitations.[1] Two-dimensional solids are described as "crystals," without conventional long-range positional order, in which phonon excitations coexist with bound dislocation pairs.[2] Rare gases physisorbed on various substrates,[3] reconstructed surfaces of metal and semiconductor crystals,[4] intercalated systems,[5] and smectic liquid crystals[6] are all examples of systems which exhibit two-dimensional characteristics. There now exists a substantial body of knowledge on crystalline order in both two and three dimensions, and it is an intriguing question as to how the nature of the order evolves as the aspect ratio and thence the effective dimensionality of the system changes.

In a fluctuating system, dimensionality is determined by the relative magnitude of the correlation lengths in the different directions. Two-dimensional behavior is expected when the correlation length in one direction is much smaller than those in the other two directions. Two-dimensional systems can be also realized by preparing thin films with infinite extension in two directions and with a finite thickness.[7] When we probe properties whose length scale is much larger than the shortest correlation length, or the physical thickness, the system is expected to show two-dimensional behavior.

Positional ordering is quantified by the density-density correlation function $G(\mathbf{r})=\langle\rho(\mathbf{r})\rho(\mathbf{0})\rangle$, where $\rho(\mathbf{r})$ is the mass density at position $\mathbf{r}$. For a three-dimensional solid, $G(\mathbf{r})$ decays to a nonzero constant at large $\mathbf{r}$, whereas it decays algebraically to zero at large $\mathbf{r}$ for a two-dimensional system.[1] The correlation function can be studied experimentally by measuring the x-ray-scattering profile. In the first Born approximation, the scattered intensity is proportional to the instantaneous structure factor $S(\mathbf{Q})$, where $S(\mathbf{Q})\sim\int d\mathbf{r}\,G(\mathbf{r})e^{i\mathbf{Q}\cdot\mathbf{r}}$. In a three-dimensional system with long-range positional order, $S(\mathbf{Q})$ is composed of δ-function Bragg peaks at reciprocal lattice vectors ($\mathbf{G}$) with diffuse $1/|\mathbf{q}|^2$ tails resulting from phonon excitations; here $\mathbf{q}=\mathbf{Q}-\mathbf{G}$ is the deviation from the reciprocal lattice vector $\mathbf{G}$. The magnitude of the thermal diffuse scattering is inversely proportional to the elastic constants of the system. For a two-dimensional system, the Bragg peaks are replaced by algebraically diverging singularities $S(\mathbf{Q})\propto 1/|\mathbf{Q}-\mathbf{G}|^{2-\eta_{\rm G}}$; resulting from the algebraically decaying correlation function. Therefore, as the dimensionality of the system is reduced from three to two, the Bragg peaks disappear, and the line shape of the diffuse scattering changes from $1/|\mathbf{Q}-\mathbf{G}|^2$ to $1/|\mathbf{Q}-\mathbf{G}|^{2-\eta_{\rm G}}$; that is, the effective value of the exponent, $\eta_{\rm eff}$, varies from 0 to $\eta_{\rm G}$. Systems in the intermediate range show a two-dimensional-like line shape for small $|\mathbf{q}|$ (probing a large length scale in real space) and presumably would show a three-dimensional line shape $1/|\mathbf{Q}-\mathbf{G}|^2$, for large $|\mathbf{q}|$, which corresponds to short length scales.

The rich phase diagrams of smectic liquid crystals have been intensively studied for decades; however, a clear physical picture of the different phases has only recently emerged.[8] In all of the smectic phases of thermotropic liquid crystals, which are usually long, rodlike molecules, the molecules are segregated into well-defined layers and the long axes of the molecules are aligned. Two of the high-temperature phases, the smectic-A (S_A) and the smectic-C (S_C) phases, are well described as stacked two-dimensional fluids, since molecules in a given layer show fluidlike ordering and the layers are only weakly coupled. As the correlation length in a smectic layer grows with decreasing temperature, the coupling between the layers increases and the system freezes into a three-

dimensional solid. The freezing transition may occur either directly or via an intermediate hexatic phase.[8,9] It is possible to make very thin smectic samples using the freely suspended film technique, as is well described in the literature.[10] In the low-temperature phases of thin smectic films, the molecules lock together between the layers, and these films may be treated as two-dimensional solids. Freely suspended films of a smectic liquid crystal provide an excellent system for the study of crystalline order as a function of effective dimensionality, since high-quality single-domain samples of various thicknesses can be made from the same material.

In this paper we present high-resolution synchrotron x-ray-scattering measurements of the crystalline phase of freely suspended films of 8OSI [racemic 4-(2′-methylbutyl)phenyl 4′-(octyloxy)-(1,1′)-biphenyl-4-carboxylate]. 8OSI has the smectic phase sequence $S_A \rightarrow S_C \rightarrow S_I \rightarrow S_J$,[11] which includes an intermediate tilted hexatic phase, S_I, and a crystalline phase, S_J. The tilt angle of the molecules with respect to the smectic layer normal is 26.5°. The lattice spacing in the smectic layer is 4.5 Å, and the layer spacing is 28.4 Å in the S_J phase. The thickness of the samples was varied from 5 molecular layers to roughly 1000 layers thick. Careful analysis of the scattering profiles of 5-, 14-, 18-, ~90-, and ~1000-layer films has demonstrated evidence of dimensional crossover.

This paper is organized as follows. In Sec. II the experimental configuration is described and the details of the instrumental resolution are discussed. In Sec. III we report the experimental results and their analysis. First, the data for the thick film, which is expected to be in the three-dimensional limit, are presented. It is shown that the S_J phase is a true crystalline phase with large-amplitude thermal fluctuations. Highly anisotropic elastic constants are obtained from the data. The line-shape analysis of the thin films is presented in the second part of this section. The amount of diffuse scattering increases as the film thickness is decreased. The change in the value η_{eff}, as a function of thickness, indicates dimensional crossover. In Sec. IV we present theoretical considerations on the amplitude of fluctuations and their correlation functions. We summarize the results of this experiment in Sec. V.

II. EXPERIMENTAL DETAILS

Single-domain films, produced by the freely suspended film technique, were used. A 1-kG magnetic field generated by a pair of $SmCo_5$ permanent magnets aligned the tilt direction of the molecules. This provided the effective ordering field to lock the direction of the local crystalline axes via the coupling between the molecular tilt and the bond orientation.[12] Applying an external magnetic field to produce single-domain samples in tilted hexatics was one of the experimental breakthroughs required to reveal the nature of the hexatic S_I and S_F phases[9,13] and is also crucial in this experiment.

Films were made in the S_A phase, at about 140° C, and slowly cooled into the S_I phase. Single-domain S_I samples produced this way then froze into a single-crystal S_J phase as the temperature was lowered further; this phenomenon was first demonstrated by Brock *et al.*[13] All the films, from 5 layers thick to ~1000 layers thick, underwent the S_I-S_J transition around 345.7 K. The transition temperature was quite insensitive to film thickness, varying by at most 0.5 K. The transition was very abrupt, suggesting that it was first order, in agreement with earlier studies.[13] The data in the crystalline phase were taken near 343.7 K, about 2 K below the transition. The diameter of the films was 6.375 mm, and the films were held inside a two-stage, temperature-controlled, oven, which was kept at a pressure of ~0.1 torr of nitrogen. The thickness of thin films less than 20 layers was determined by the width of the x-ray-scattering profile perpendicular to the smectic layers, although optical reflectivity measurements were used as a guide prior to the x-ray measurement.

The x-ray-scattering profile for momentum transfers perpendicular to the smectic layers is similar to the optical diffraction pattern from a finite number of slits. The width of the diffraction maxima is determined by both the finite number of smectic layers and the mosaic distribution of the smectic layer normals. For thicker films the width decreases and the mosaic distribution of the layer normal becomes more important, and so must be deconvolved; this introduces large uncertainties in the thickness measurement. We use the relative phase angle of the ordinary and extraordinary rays of an initially linearly polarized laser beam induced by the birefringence of 8OSI as it passes through the film to measure the thicknesses of the thick films. Details of the optical technique are discussed elsewhere.[14]

The experiments were performed at the IBM/MIT beam line X-20A at the National Synchrotron Light Source (NSLS) at Brookhaven National Laboratory. The white x-ray beam from a bending magnet is focused by a platinum-coated Si(111) mirror and monochromatized by a pair of asymmetrically cut Ge(111) crystals. Using asymmetric Ge crystals allows us to match the angular acceptance of our monochromator system to the angular divergence of the source. The double-crystal monochromator results in an incoming beam resolution profile with tails which fall off as q^{-4}. The size of the beam is set by an aperture in a tantalum plate in front of the sample cell. The scattered x-ray beam from the sample is then analyzed by a flat Ge(111) crystal and two pairs of slits. Figure 1 depicts schematically the scattering geometry used.

The spectrometer resolution in the scattering plane is constructed from the incoming and the outgoing resolutions. For a given angular divergence of the incident x rays, $R_1(\theta)$, and an outgoing acceptance $R_2(\Theta)$, the resolution function $R(\theta,\Theta)$ at the point in angle space (θ_0,Θ_0) is given by

$$R(\theta,\Theta)=R_1(\theta-\theta_0)R_2(\Theta-\Theta_0+\theta-\theta_0)\ . \tag{1}$$

This equation represents the measured intensity distribution in the scattering plane from a δ-function scatterer at the sample position. The resolution function in reciprocal-lattice coordinates is obtained by a transfor-

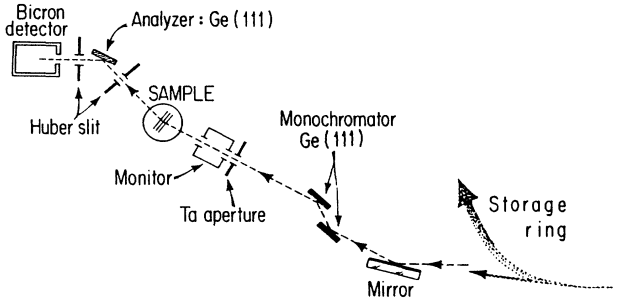

FIG. 1. Experimental geometry used in the experiment.

mation from (θ,Θ) to (K,L). The definitions of angles and the coordinates are given in the top part of Fig. 2.

The resolution function is measured by placing a Si(111) single crystal at the sample position. The rocking curves of the sample crystal and detector are used to obtain the incoming divergence of the x-ray beam and the outgoing acceptance of the detector separately. It is essential to deconvolve the intrinsic Darwin curve of the Si(111) crystal to obtain the exact incoming and outgoing resolutions from the measured rocking curves.[15] Upon deconvolution we find that a Lorentzian line shape raised to the power of 1.36 with a 0.0017° half width at half maximum (HWHM) describes the incoming divergence of the beam quite well, while the outgoing resolution is well described by a Lorentzian with a 0.0023° HWHM. Figure 2(a) shows the measured data, while Fig. 2(b) gives the resultant resolution contour in the scattering plane. Because of the configuration of the monochromator and the analyzer crystals, the resolution function has a tilted and elongated shape, with a sharply decaying tail along the incoming direction and a relatively slowly decaying tail along the outgoing direction. A cut along $L=0$ can be thought of as the longitudinal resolution, along the direction connecting the origin to the peak in the reciprocal space, and one along $K=0$ as the transverse resolution in the scattering plane. The longitudinal resolution has a width of 2.7×10^{-4} Å^{-1} HWHM, while the transverse resolution is 5.4×10^{-5} Å^{-1} wide (HWHM). The resolution function in the scattering plane has tails which are empirically described by the form $1/|\mathbf{q}|^{4.7}$ along both axes. The resolution perpendicular to the planes is determined by slits. It is well described by a Gaussian; for the thick film, the out-of-plane resolution was 0.0015 Å^{-1} HWHM, while it was set at the coarser value 0.015 Å^{-1} HWHM for all of the thin-film measurements.

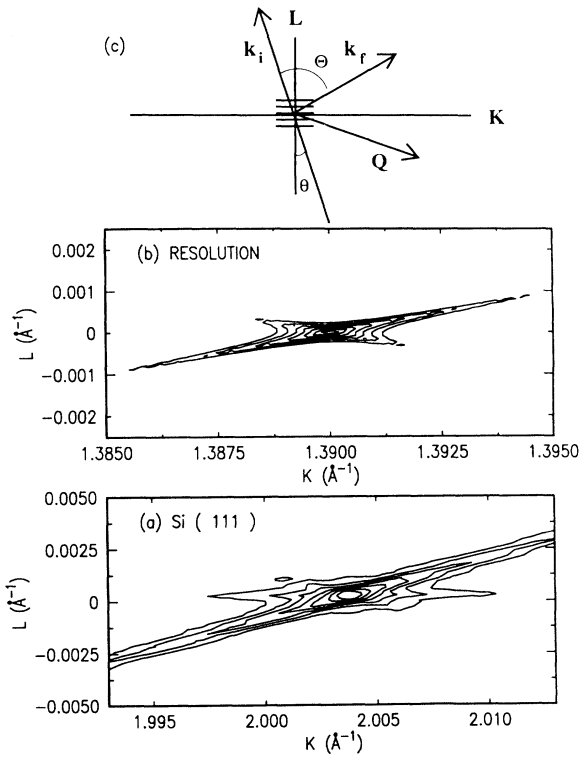

FIG. 2. (a) Scattering profile from a Si(111) single crystal in the scattering plane. (b) Resolution function in the scattering plane generated from the separately measured incoming divergence of the beam and outgoing acceptance of the detector. Note that different scales are used in the two figures. (c) Incoming and outgoing directions of the x-ray beam relative to the smectic layer normal, which is defined to be the L direction in the reciprocal-lattice coordinate system.

The tilted, elongated resolution function makes the measured intensity profile complex. If the intrinsic scattering from a sample is a δ rod, that is, very sharp longitudinally, but flat in the transverse direction, as is the case for a two-dimensional crystal with L in the direction perpendicular to the plane, then a longitudinal scan does not simply show the cut along $L=0$ in Fig. 2; rather it integrates over the intensity along the spine of the elongated shape, which is quite broad with slowly decaying tails. For this reason the broadening in the transverse direction must be considered carefully in the analysis of the longitudinal scans.

III. RESULTS AND ANALYSIS

A. Thick film: Three-dimensional limit

There are two major reasons for studying the crystalline order of a 3D sample. First, by studying a thick sample, questions about the nature of the bulk liquid-crystal S_J phase, such as the existence of true long-range order, elastic properties and stacking order can be addressed. The coupling constants between molecules deduced from the elastic properties may be useful in constructing models for thinner samples or systems close to the 2D limit. Second, a thick film provides the 3D limit of the dimensional crossover to be used as a reference for the thin-film data. Both these reasons require a high-quality single-domain sample and precise knowledge of the instrumental resolution.

We successfully grew such a sample, whose thickness was measured by the optical technique to be ~3 μm. The scattered intensity from this thick sample was sufficiently large that we were able to reduce our x-ray spot size to a diameter of 0.1 mm by means of a tantalum

aperture in front of the sample chamber and thence improve the observed mosaic structure. The out-of-scattering-plane resolution was set to 0.1° HWHM by slits with a 0.1-mm opening. The mosaicity, the distribution of the crystalline axes in the smectic layers, was found to be better than 0.1°, and the mosaic distribution of the smectic layer normal was about 0.01°.

The scattering profile of the thick film consists of a sharp Bragg component, as occurs in conventional solids, and a large amount of thermal diffuse scattering. Figure 3 shows the scattering profiles along the longitudinal direction $(0, G_{010}+q_\perp, 0)$ (see top of Fig. 1) and the transverse direction $(0, G_{010}, q_z)$ around the first reciprocal lattice vector $(0, G_{010}, 0)$. The transverse scan is in the direction perpendicular to the smectic layers. The high flux of the synchrotron beam coupled with the sharp resolution allows us to measure the scattered intensity over six orders of magnitude for a two-decade change in $|\mathbf{q}|$. The diffuse scattering from the thick film is highly anisotropic. There is approximately two orders of magnitude more diffuse scattering in the transverse direction than in the longitudinal direction for the same $|\mathbf{q}|$. This indicates that phonons in the transverse direction are excited much more easily.

Although the scattering profile perpendicular to the smectic plane, along the $(0, G_{010}, q_z)$ direction (transverse scan), is extremely sharp ($\sim 2\times 10^{-4}$ Å^{-1} HWHM), there is some mosaic structure, which determines the line shape near the center. The mosaic distribution of the smectic layer normal, measured by a transverse scan, can be described empirically by a Lorentzian raised to some power:

$$\frac{A}{(1+|\mathbf{q}|^2/\kappa^2)^\phi}\ , \tag{2}$$

with $\kappa = 0.000\,18$ Å^{-1} and $\phi = 1.64$. The broadening of the transverse scan due to this mosaic spread induces broadening in the longitudinal direction through the tilted shape of the resolution function as discussed in Sec. II. Indeed, the central part of the longitudinal scan, whose width is about 3×10^{-4} Å^{-1}, turns out to be very well described by the effects of the resolution function convolved with the mosaic spread in the transverse direction; that is, no intrinsic longitudinal width is observed to within our experimental precision. This clearly demonstrates that the main contribution to the intrinsic scattering near the peak is from a δ-function-like Bragg component.

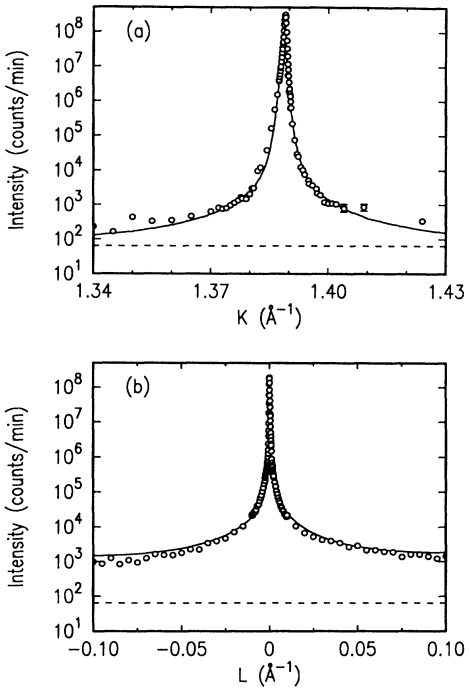

FIG. 3. (a) Longitudinal scan in the thick film. (b) Transverse scan in the thick film. The thick solid lines in both cases are the result of fits to Eq. (6). The background levels are represented by the broken lines. The intensities are normalized to a ring current of 100 mA.

To explain the scattering quantitatively, we use first-order thermal diffuse scattering as predicted by harmonic phonon theory:[16]

$$S(\mathbf{Q}) = e^{-2W}|F(\mathbf{Q})|^2 \sum_R e^{i\mathbf{Q}\cdot\mathbf{R}} \left[1+\sum_q e^{i\mathbf{q}\cdot\mathbf{R}} \sum_{i,\alpha=1}^{3} Q_i^2 \langle u_{1,\alpha}(\mathbf{q})^2\rangle\right]\ . \tag{3}$$

Here e^{-2W} is the Debye-Waller factor, $F(\mathbf{Q})$ is the molecular form factor, $\mathbf{Q}$ is the scattering vector, and $\mathbf{u}_\alpha(\mathbf{q})$ is the displacement vector of the αth phonon mode with wave vector $\mathbf{q}$. Along the high-symmetry directions of the crystal, such as the $(0, G_{010}+q_\perp, 0)$ and $(0, G_{010}, q_z)$ directions, phonons can be classified as either purely longitudinal or purely transverse, and the scattering profile simplifies to

$$\begin{bmatrix} S(q_z) \\ S(q_\perp) \end{bmatrix} = e^{-2W}|F(\mathbf{Q})|^2 \frac{(2\pi)^3}{\Omega_0} \left[\delta(\mathbf{q}) + \frac{V_0}{(2\pi)^3} G_{010}^2 \begin{bmatrix} u_t^2(00q_z) \\ u_1^2(0q_\perp 0) \end{bmatrix}\right]\ , \tag{4}$$

where u_t and u_1 are, respectively, the transverse and longitudinal displacements in the [010] direction; Ω_0 is the volume of the unit cell and V_0 the volume of the crystal. Using the equipartition theorem,[16]

$$\langle |u_\alpha(\mathbf{q})|^2\rangle = \frac{k_B T}{NM\omega_\alpha^2(\mathbf{q})}\ , \tag{5}$$

where N is the number of molecules and M is the mass of a molecule, and with the assumption that $\omega_\alpha = V_\alpha q$ for small q (V_α is the sound velocity), one can see that the structure factor along the high-symmetry directions is composed of a δ-

function peak with $1/q^2$ thermal diffuse tails. In a low-symmetry direction, the normal modes of the system no longer have purely longitudinal or transverse polarizations, and the expression for the structure factor becomes more complicated. We have assumed for simplicity that the structure factor along an arbitrary direction has the anisotropic form

$$S(\mathbf{Q})=e^{-2W}|F(\mathbf{Q})|^2\frac{(2\pi)^3}{\Omega_0}\left[\delta(\mathbf{q})+\frac{k_BTG_{010}^2}{(2\pi)^3\rho V_1^2}\frac{1}{q_\perp^2+(V_t^2/V_1^2)q_z^2}\right], \tag{6}$$

where ρ is the density of the system. This was constructed to reduce to the exact results in the longitudinal and transverse directions.

The measured scattering profiles along the longitudinal and transverse directions are fit to a convolution of Eq. (6) with the resolution function given in Sec. II:

$$I(\mathbf{Q})=I_0\left[\int d\mathbf{q}'S(\mathbf{q}')R(\mathbf{Q}-\mathbf{q}')\right]+I_{\mathrm{BG}}\ , \tag{7}$$

where I_0 is the overall amplitude and I_{BG} is the measured background. The integration in the scattering plane was performed numerically, while that in the out-of-scattering-plane direction was carried out analytically. As may be seen in Fig. 3, Eq. (7) describes the measured line shape in the longitudinal and transverse directions extremely well, justifying the construction used for the structure factor.

From these fits we have obtained the elastic stiffness constants $\rho V_l^2=1.4\times10^8$ $(\pm3\times10^7)$ N/m^2 and $\rho V_t^2=2.0\times10^6$ $(\pm1.8\times10^5)$ N/m^2. The transverse sound velocity is only about 12% of the longitudinal velocity, emphasizing the highly anisotropic nature of the system. These elastic stiffness constants, especially along the transverse direction, are very small compared to those of conventional crystals,[17] which indicates that the S_J phase is a "soft" crystalline phase. They are only about one-quarter of those in the S_G phase of TBBA (terephthal-bis-butyl-alkylaniline), which has a crystal structure closely related to that of the S_J phase.[18] Despite this large difference, it is noteworthy that the ratios between the transverse and longitudinal sound velocities of the two systems are comparable, indicating that this small interlayer coupling may be common to all smectic systems. A possible explanation of the small values of the measured elastic constants of 8OSI, relative to TBBA, is that our data were taken just 2 K below the melting point, whereas the TBBA data in Ref. 18 were taken about 25 K below the phase transition. In support of this statement, the transverse elastic stiffness constant in the TBPA (terephthal-bis-pental-alkylaniline) system shows a marked rise below the transition.[9] As a note of caution, we should also remark that in the analysis we have ignored possible sources of diffuse scattering other than thermal fluctuations. Inclusion of other sources, such as finite-size effects, acts so as to increase the deduced values of the elastic constants.

The thick-film results may be summarized as follows. A Bragg δ-function component is necessary to describe the scattering profile, implying that there is long-range positional order; this demonstrates that a film 3 μm thick is in the 3D limit, at least as probed by our high-resolution measurements. The $|q|^{-2}$-dependent thermal diffuse scattering is also a feature of three-dimensional systems. The smallness of the transverse sound velocity implies that there are large harmonic fluctuations in the interplanar order, although the sharp Bragg peak demonstrates that the long-range stacking order of the smectic layer persists.

B. Thin films

As the film thickness is decreased, the scattering begins to take on a more two-dimensional character. First, the scattering profile in the transverse direction becomes broad, showing the rodlike scattering characteristic of a two-dimensional system. The scattering profile is as sharp as the instrumental resolution in the smectic plane, but is broad in the direction perpendicular to the smectic layers. The widths of the transverse scans are used to determine the thicknesses of the films by approximating their central regions to "N-slit diffraction patterns."

Second, the intensity in the diffuse wings of the longitudinal scans increases relative to the peak intensity as the thickness decreases, which indicates that the amplitude of the thermal fluctuations is increasing. This is illustrated in Fig. 4, in which the raw data, background subtract-

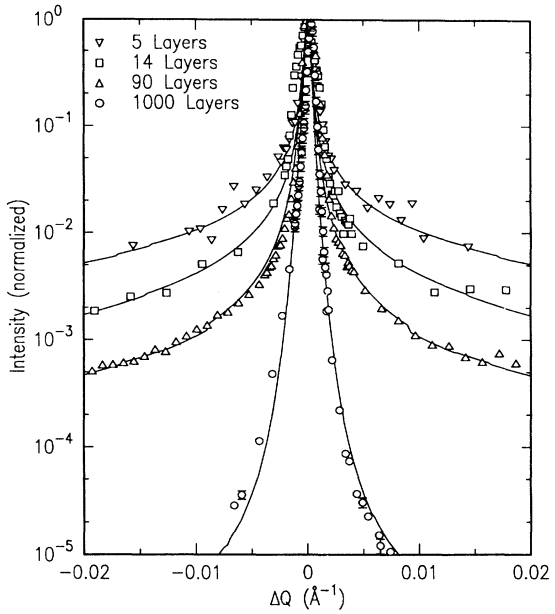

FIG. 4. Longitudinal scans from films of various thicknesses. The data are background subtracted and normalized to the peak intensity in order to compare the peak-to-tail intensity ratio. The solid lines are the results of fits to Eq. (9) for films thinner than 100 layers and to Eq. (6) for the 1000-layer film. Note that both the mosaicity and instrumental resolution are much narrower for the 1000-layer film compared with those for the thin films. This decreases the relative intensity of the tails for the thick film. The glitches in the solid lines are due to the sharp cutoff of the resolution function by the slits.

ed and normalized to the peak values, are plotted. To compare the intrinsic intensities, the effect of the resolution volume, which was smaller by a factor of 10 for the thick film because of the small spot size and narrow slits in the out-of-scattering-plane direction, has to be deconvolved, and varying mosaicities must be taken into account. The measured diffuse intensity is roughly proportional to the resolution volume, while the peak value is independent of it. It is clear, nevertheless, from Fig. 4 that the relative intensity in the wings varies by orders of magnitude as the sample thickness is changed.

Experimentally, it was observed that for films of thickness of less than 20 layers, radiation damage was a significant problem. The low scattering power of thin films means that, in order to obtain reasonable statistics, long counting times must be used. After a sample has been exposed to the intense synchrotron x-ray beam for times in excess of a couple of hours, the peak intensity of a scan decreases dramatically. To ensure consistent data, the peak intensity was measured after each scan to monitor the effects of radiation damage.

As the film thickness decreases, the in-plane mosaicity becomes broader. This is partly due to the relatively large x-ray spot size used to compensate for the small signal rate. However, we believe that the large amplitude of the bond orientational fluctuations in the thin-film hexatic phase also contributes to this broadening in the solid phase.[19] Specifically, these fluctuations heuristically correspond to a mosaic distribution of the in-plane crystalline axes, which is, in part, frozen into the crystalline phase at the first-order hexatic-solid freezing transition.

To characterize quantitatively the systematic changes of the line shape as the sample thickness decreases, we have approximated the intrinsic line shape of a thin film to that of an idealized two-dimensional system:

$$S(\mathbf{Q}) \propto f(Q_z) \frac{1}{(\mathbf{Q}_\perp - \mathbf{G})^{2-\eta_{\text{eff}}}} , \tag{8}$$

in which the absence of true long-range order is assumed. Note that $f(Q_z)$, the Q_z dependence of the scattering function, is assumed separable from the in-plane component of the structure factor. This is exact for a true two-dimensional system; in that case, $f(Q_z)$ is simply the molecular form factor in the $\mathbf{Q}_z$ direction. We note, however, that in three dimensions the structure factor is nonseparable as described in Sec. III A [Eq. (6)].

The transverse scans of thin films perpendicular to the layers are illustrated in Fig. 5. The peaks become broader as the sample thickness decreases, showing the effect of the films' finite size. The central parts of the scans are approximated to N-slit diffraction patterns to obtain the sample thicknesses. The positions of the higher-order Bragg peaks show that the S_J phase of 8OSI has the rare AA-type stacking order of the smectic layers.[10] Even though this stacking order exists, the amplitude of the stacking fluctuations is so great that no subsidiary peaks are observed between the Bragg peaks. The subsidiary peaks, which exist between the principal peaks in the N-slit diffraction pattern, have been observed in the $(0,0,q_z)$ direction,[20] where layer compression modes are

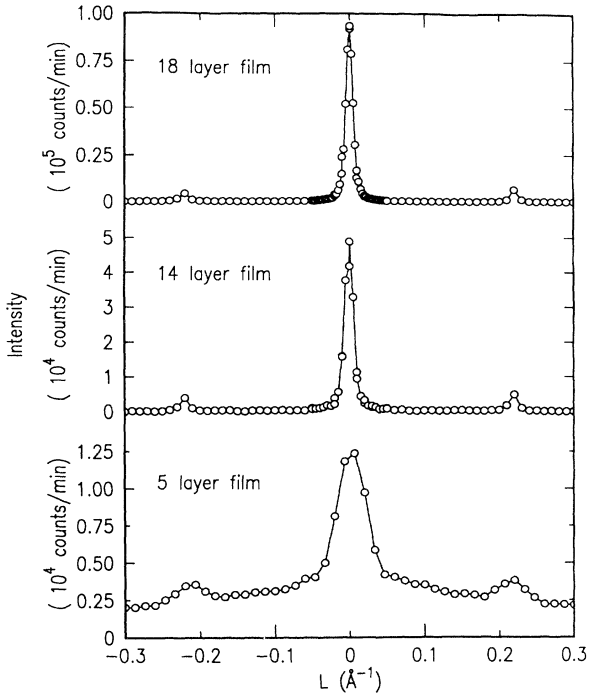

FIG. 5. Transverse scans from 5-, 14-, and 18-layer films. The thicknesses of the samples are derived from the widths of the peaks. The solid lines are guides to the eye. The intensities are normalized to a ring current of 100 mA.

important, but fluctuations in the stacking order are irrelevant. Therefore, we conclude that since layer compression fluctuations are not enough to decrease significantly the intensity of the secondary peaks, the layer slipping fluctuations must represent the dominant contribution to the diffuse scattering in the $(0,G_{010},q_z)$ direction.

For the longitudinal line-shape analysis, the broadening of the transverse scans and in-plane mosaic structure must be treated properly. The in-plane mosaicity is measured by performing an in-plane angular scan; the proper mosaic average is then done as part of the analysis. After mosaic averaging, the resolution function in the scattering plane, discussed in Sec. II, is convolved with the intrinsic $S(\mathbf{Q})$ [Eq. (8)] to describe the measured scattering profile.

The final functional form of the measured intensity in the longitudinal direction can be summarized as

$$I(0,Q_k,0) = I_0 \int dq_k' \left[\int dq_z' R(q_k',q_z') f(q_z') \times \int d\chi \frac{M(\chi)}{(\mathbf{Q}-\mathbf{G})^{2-\eta_{\text{eff}}}} \right] + I_{\text{BG}} , \tag{9}$$

where $M(\chi)$ is the measured in-plane mosaic structure and I_{BG} is the background scattering. We have fit the data in the range $|\mathbf{q}| < 0.05$ Å^{-1}. Outside this region the statistics are too poor to make the data useful. The back-

ground scattering is fixed at the value measured far from the peak, at $|\mathbf{q}|=0.2$ Å^{-1}. It is important to measure the background directly since in the fitting routine the value of the exponent η_{eff} is strongly coupled to I_{BG}. All of the integrations have been done using elaborate numerical methods, paying close attention to the divergence at the peak position. Even though the assumption of separability is incorrect as we approach the 3D limit, the functional form has been applied to the thick-film data to keep the analysis consistent throughout the data set.

Figure 6 shows the longitudinal scan data together with the results of fits to Eq. (9). The adjustable parameters in the fits are the overall amplitude, the peak position, and η_{eff}, with only η_{eff} influencing the shape of the curves. Considering this, we believe that the fits are excellent. We have plotted the resulting values of η_{eff} in Fig. 7. The thinnest film, which is five molecular layers in thickness, has $\eta_{\text{eff}}=0.18\pm0.013$. For the next thinnest film, which is 14 layers thick, η_{eff} shows a dramatic drop to less than 0.1. The thickest film (~ 3 μm thick) has $\eta_{\text{eff}}=0.001\,46\pm0.000\,64$, showing that the value of η_{eff} does indeed approach zero with increasing thickness, as it must do.

Although the data were taken at just 2 K below the transition, the smallness of the value of η_{eff} compared to the predicted value of $\frac{1}{3}$ for a 2D Kosterlitz-Thouless melting transition[2,21] suggests that the role of the dislocations is minor. This, presumably, is connected with the fact that the melting transition is first order. From the extrapolation of the behavior of η_{eff} in Fig. 7, one might guess that η_{eff} for films thinner than five layers would be close to, or larger than, $\frac{1}{3}$. As η_{eff} approaches $\frac{1}{3}$, dislocations become increasingly important, and one must consider their effects, such as renormalizing the elastic constants and giving rise to a continuous, rather than first-order, melting transition.[2,21]

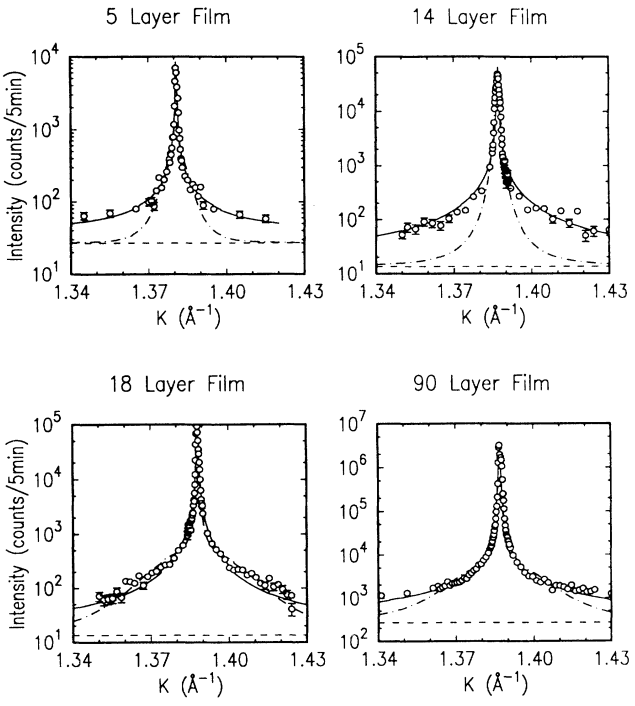

FIG. 6. Longitudinal scans in 5-, 14-, 18-, 90-, and 1000-layer films. The solid lines are the results of the fit to Eq. (9), while the broken lines are the results of the fit to the convolution of the resolution and Eq. (10). The dotted straight lines are the measured backgrounds. The intensities are normalized to a ring current of 100 mA.

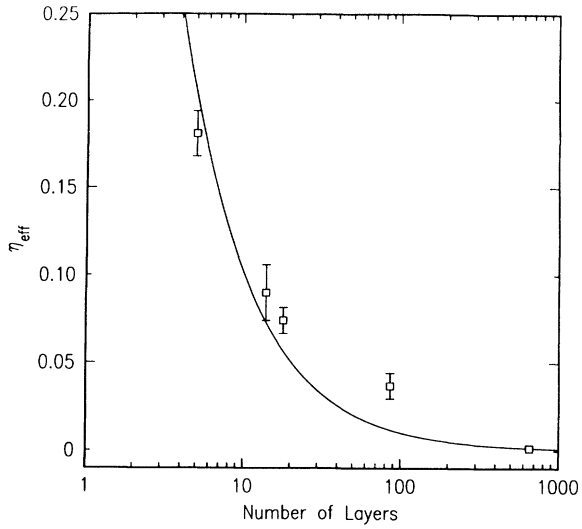

FIG. 7. η_{eff} obtained as a result of the fit to Eq. (9). The solid line is a fit to $\propto 1/P$, where P is the number of layers.

The primary physics underlying Eq. (8) is the nonexistence of true long-range order. As a check on this assumption, we have carried out fits to a line shape deriving from an assumed lattice structure in the smectic layers, that is, a line shape with a 2D Bragg component and $1/q_{\perp}^2$ tails. A well-defined lattice is only possible in 2D for a finite system. In this case we have assumed that the $1/q^2$ tails may be replaced by a Lorentzian whose width is roughly the inverse of the sample size. Accordingly, we have tried to fit the data to a line shape composed of a two-dimensional δ function in the smectic planes, with thermal tails represented by a two-dimensional Lorentzian:

$$S(\mathbf{Q})=I_0 f(Q_z)\left[\delta(\mathbf{Q}_{\perp})+\frac{I_{\text{TDS}}}{(\mathbf{Q}-\mathbf{G}_{010})^2+\kappa^2}\right]+I_{\text{BG}}\ . \quad (10)$$

The background is fixed to the same value used in Eq. (9). As shown in Fig. 6, Eq. (10), convoluted with the resolution function including the mosaicity, clearly does not describe the data as well as Eq. (9). In particular, as the films get thinner, Eq. (10) cannot explain the large amount of diffuse scattering. Even for the 18-layer film, which Eq. (10) describes reasonably well, Eq. (9) nevertheless gives a somewhat better fit as judged by a smaller χ^2. Thin films are thus much better described by a power-law divergence than a line shape with a δ-function peak and diffuse tails, confirming our assumption that there is no true long-range order.

IV. THEORETICAL CONSIDERATIONS

In this section we reconsider the amplitude of the fluctuations and their correlations, explicitly including the finite thickness of the film. We consider only the phonon contribution; this is justified by the smallness of the values of η_{eff} as discussed in Sec. III. The position of an individual particle is written as $\mathbf{X}_i=\mathbf{R}_i+\mathbf{u}_i$, where the $\mathbf{R}_i$'s form a bravais lattice, and $\mathbf{u}_i$ is the deviation from the equilibrium position. For an N-particle system, the mean-square amplitude of the fluctuations in the harmonic approximation is given by

$$\langle |\mathbf{u}_i|^2 \rangle = \frac{1}{N} \frac{k_B T}{M c_j^2} \sum_{\mathbf{q}} \frac{1}{|\mathbf{q}|^2} , \tag{11}$$

where c_j is an effective sound velocity which can be expressed as a combination of the elastic constants. Performing the summation in two and three dimensions, respectively, the mean-square amplitude of the deviation is given by

$$\langle |\mathbf{u}_i|^2 \rangle = \begin{cases} \dfrac{k_B T}{M c_j^2} \dfrac{a^2}{2\pi} \ln\left[\dfrac{L}{a}\right] & \text{(2D)} \\ \dfrac{k_B T}{M c_j^2} \dfrac{a^2}{2\pi} & \text{(3D)}, \end{cases} \tag{12}$$

where a is the lattice spacing and L is the linear dimension of the system. In two dimensions, the mean-square fluctuations diverge with the size of system, radically different from the situation in three dimensions, where they are a fraction of the lattice spacing. As is well known, the diverging amplitude of the fluctuations in two dimensions formally destroys true long-range order for an infinite system. However, for a finite-size system $\langle |\mathbf{u}_i|^2 \rangle^{1/2}$ can be smaller than the lattice spacing, because of its slow logarithmic divergence.

For a system with finite thickness, specifically one with P layers, $\langle |\mathbf{u}_i|^2 \rangle$ is calculated by breaking the summation $\sum_{\mathbf{q}}$ into $\sum_{\mathbf{q}_\perp} \sum_{q_z}$:

$$\langle |\mathbf{u}_i|^2 \rangle = \frac{k_B T}{M c_j^2} \frac{a^2}{2\pi} \left[\frac{1}{P} \ln\left[\frac{L}{a}\right] + \frac{1}{P} \sum_{q_z \neq 0} \ln\left[1+\frac{(\pi/a)^2}{q_z^2}\right] \right] . \tag{13}$$

The first term is from the Fourier components with $q_z=0$, and the second term, which contains the summation over $\sum_{q_z \neq 0}$ is approximately equal to unity. Here we have used the same elastic constant in all directions in order to obtain an intuitive understanding of the physics, without complicating the algebra. For the modes with $q_z=0$, the molecules in one layer remain fixed with respect to all other layers; hence the coupling between these extended molecules, stretching across all layers, is P times as strong as that between the bare molecules. The fluctuations of these $q_z=0$ modes are reduced in amplitude relative to those in Eq. (12), and this manifests itself in Eq. (13) by the fact that for these modes the elastic constants have been effectively renormalized by a factor P. From Eq. (13) one can roughly estimate the thickness of a sample for which the amplitude of the fluctuations is of the same order as those of a three-dimensional system. For a 2D system of 1 cm diameter, the amplitude of the fluctuations is less than twice as large as those in a 3D system for $P=17$, suggesting that the crossover from 2D to 3D behavior occurs for relatively small thicknesses.

The detailed behavior of a system can be understood by considering the correlation function

$$\begin{aligned} G(\mathbf{r}) &= \langle \rho(\mathbf{r})\rho(\mathbf{0}) \rangle \\ &= \langle e^{i\mathbf{G}\cdot[\mathbf{u}(\mathbf{r})-\mathbf{u}(\mathbf{0})]} \rangle . \end{aligned} \tag{14}$$

After some algebra, the correlation function in two and three dimensions is given by

$$G(\mathbf{r}) \propto \begin{cases} \dfrac{1}{\mathbf{r}^{\eta_G}} \quad \text{with } \eta_G = \dfrac{k_B T a^2 |\mathbf{G}|^2}{2\pi M c^2} & \text{(2D)} \\ \exp\left[\dfrac{k_B T a^2 |\mathbf{G}|^2}{4\pi M c^2} \dfrac{|\mathbf{a}|}{|\mathbf{r}|} \right] & \text{(3D)}. \end{cases} \tag{15}$$

The behavior of the correlation function of a system with finite thickness varies according to the region of interest. For length scales smaller than the thickness of the sample, the functional form is quite complicated;[7] however, for large length scales, the system shows the characteristics of a two-dimensional system, with the exponent η reduced in exactly the same way as the mean-square fluctuations were reduced by the renormalized elastic constant, and the correlation function is given by

$$G(\boldsymbol{\rho},0) \propto \frac{1}{|\boldsymbol{\rho}|^{\eta_G/P}} , \tag{16}$$

that is, $\eta_{\text{eff}}=\eta_G/P$. Here $\boldsymbol{\rho}$ is the in-plane component of $\mathbf{r}$. This equation holds only when $|\boldsymbol{\rho}|$ is much larger than the thickness of the sample. The detailed derivation of this correlation function is given in Ref. 7 in the context of thin-film superconductors. Even with the simple arguments used, the predicted $1/P$ dependence of η_{eff} gives rough qualitative agreement with our observed values as illustrated in Fig. 7. As expected, the agreement worsens for thicker films when the contributions of the $q_z \neq 0$ modes become important; though, of course, it has the correct 3D limit.

V. DISCUSSION AND CONCLUDING REMARKS

Two-dimensional line shapes, which assume the separability of the q_z dependence from the in-plane component of the structure factor, have been used to describe the thin-film data; this is equivalent to ignoring all the excitations with $q_z \neq 0$. Such behavior is not strictly correct for a system with nonzero thickness, and in principle the x-ray-scattering profile should show 2D behavior near the reciprocal vectors, crossing over to 3D behavior with increasing $|\mathbf{q}|$. However, this crossover is very subtle, and analyzing the data in this manner introduces too many fitting parameters to extract any meaningful information. We have instead characterized the profiles for finite-thickness films by a power-law line shape with an effective exponent η_{eff}. Empirically, this form works very well.

In summary, we have observed evidence of dimensional crossover through a detailed line-shape analysis of the x-ray-scattering profiles from films of various thicknesses. The crystalline phase of the thick film is well described by conventional long-range order with large amplitude thermal fluctuations. The large amount of diffuse scattering indicates that the 3D S_J phase is a very soft crystalline phase. Elastic stiffness constants are obtained as the result of a fit to the first-order thermal diffuse scattering profile. They are small compared to those of conventional crystals.

The nature of the "crystalline" phase of thin films is more subtle. We have shown that the power-law line shape, which is characteristic of two-dimensional systems, works well for thin films. To extract the intrinsic behavior of the effective exponent η_{eff}, the instrumental resolution has been deconvolved carefully. The change of η_{eff} as a function of the thickness dramatically exhibits dimensional crossover phenomena, at least qualitatively. η_{eff} of a 5-layer-thick film is about 0.19, whereas for a $\sim$1000-layer-thick film η_{eff} is about 0.0014; that is, the thick film has $1/|\mathbf{q}|^2$ tails as one expects from harmonic phonon theory.

ACKNOWLEDGMENTS

We are grateful to J. Liang for providing the sample material. The 8OSI used in this experiment was synthesized at Tektronix Incorporated. Details of sample synthesis are described in Ref. 19. We acknowledge both MIT and IBM members for their contributions in building the beam lines X-20 at the National Synchrotron Light Source. It is a pleasure to acknowledge helpful discussions with M. Kardar. We also express our thanks to K. Blum for his assistance during the synchrotron run. This experiment was supported by National Science Foundation Materials Research Laboratory under Contract No. DMR 87-19217.

---

*Current address: School of Applied and Engineering Physics, Cornell University, Ithaca, New York 14853.

†Current address: Research Establishment Risö, Roskilde, DK-4000, Denmark.

[1]R. E. Peierls, Helv. Phys. Acta. Suppl. **7**, 81 (1934); L. D. Landau, in *Collected Papers of L. D. Landau,* edited by D. ter Haar (Gordon and Breach, New York, 1915), p. 209; N. D. Mermin, Phys. Rev. **176**, 250 (1968).

[2]D. R. Nelson and B. I. Halperin, Phys. Rev. B **19**, 2457 (1979).

[3]For a review, see R. J. Birgeneau and P. M. Horn, Science **232**, 329 (1986).

[4]P. Bak, Solid State Commun. **32**, 581 (1979).

[5]S. G. J. Mochrie, A. R. Kortan, P. M. Horn, and R. J. Birgeneau, Z. Phys. **62**, 79 (1985).

[6]D. E. Moncton and R. Pindak, Phys. Rev. Lett. **43**, 701 (1979); R. Pindak and D. E. Moncton, Phys. Today **35** (5), 57 (1982).

[7]H. J. Mikeska and H. Schmidt, J. Low Temp. Phys. **2**, 371 (1979).

[8]P. G. de Gennes, *The Physics of Liquid Crystals* (Oxford University Press, London, 1974); P. S. Pershan, *Structure of Liquid Crystal Phases* (World Scientific, Singapore, 1988); J. D. Brock, R. J. Birgeneau, J. D. Litster, and A. Aharony, Contemp. Phys. **30**, 321 (1989).

[9]D. Y. Noh, J. D. Brock, J. D. Litster, R. J. Birgeneau, and J. W. Goodby, Phys. Rev. B **40**, 4920 (1989).

[10]J. Collett, L. B. Sorensen, P. S. Pershan, and J. Als-Nielsen, Phys. Rev. A **32**, 1036 (1985).

[11]A. J. Leadbetter, J. P. Gaughan, B. Kelly, G. W. Gray, and J. Goodby, J. Phys. (Paris) Colloq. **40**, C3-178 (1979).

[12]D. R. Nelson and B. I. Halperin, Phys. Rev. B **21**, 5321 (1980).

[13]J. D. Brock, A. Aharony, R. J. Birgeneau, K. W. Evans-Lutterodt, J. D. Litster, P. M. Horn, G. B. Stephenson, and A. R. Tajbakhsh, Phys. Rev. Lett. **57**, 98 (1986); J. D. Brock, D. Y. Noh, B. R. McClain, J. D. Litster, R. J. Birgeneau, A. Aharony, P. M. Horn, and J. C. Liang, Z. Phys. B **74**, 197 (1989).

[14]E. B. Sirota, P. S. Pershan, L. B. Sorensen, and J. Collett, Phys. Rev. A **36**, 2890 (1987).

[15]J. H. Beaumont and M. Hart, J. Phys. E **7**, 823 (1974).

[16]B. E. Warren, *X-Ray Diffraction* (Addison-Wesley, Reading, MA, 1969), Chap. 11.

[17]For typical values, see N. W. Ashcroft and N. D. Mermin, *Solid State Physics* (Sanders College, Philadelphia, 1976), Chap. 22.

[18]A. M. Levelut, F. Moussa, J. Doucet, J. J. Benattar, M. Lambert, and B. Dorner, J. Phys. (Paris) **42**, 1651 (1981).

[19]J. D. Brock, D. Y. Noh, B. R. McClain, J. D. Litster, R. J. Birgeneau, A. Aharony, P. M. Horn, and J. C. Liang, Z. Phys. B **74**, 197 (1989).

[20]D. J. Tweet, R. Holiest, B. D. Swainish, H. Straggler, and L. B. Sorensen, Phys. Rev. Lett. **65**, 2157 (1990).

[21]J. M. Kosterlitz and D. J. Thouless, J. Phys. C **6**, 1181 (1973).